

Article

An Improved Genetic Algorithm for Optimal Stationary Energy Storage System Locating and Sizing

Bin Wang ^{1,*}, Zhongping Yang ¹, Fei Lin ¹ and Wei Zhao ²

¹ School of Electrical Engineering, Beijing Jiaotong University, No.3 Shangyuancun, Beijing 100044, China; E-Mails: zhpyang@bjtu.edu.cn (Z.Y.); flin@bjtu.edu.cn (F.L.)

² Beijing Metro R&D Center, Beijing 100044, China; E-Mail: dtclsb@gmail.com

* Author to whom correspondence should be addressed; E-Mail: 12121547@bjtu.edu.cn.

External Editor: Sheng Zhang

Received: 3 July 2014; in revised form: 11 August 2014 / Accepted: 19 September 2014 /

Published: 9 October 2014

Abstract: The application of a stationary ultra-capacitor energy storage system (ESS) in urban rail transit allows for the recuperation of vehicle braking energy for increasing energy savings as well as for a better vehicle voltage profile. This paper aims to obtain the best energy savings and voltage profile by optimizing the location and size of ultra-capacitors. This paper firstly raises the optimization objective functions from the perspectives of energy savings, regenerative braking cancellation and installation cost, respectively. Then, proper mathematical models of the DC (direct current) traction power supply system are established to simulate the electrical load-flow of the traction supply network, and the optimization objections are evaluated in the example of a Chinese metro line. Ultimately, a methodology for optimal ultra-capacitor energy storage system locating and sizing is put forward based on the improved genetic algorithm. The optimized result shows that certain preferable and compromised schemes of ESSs' location and size can be obtained, acting as a compromise between satisfying better energy savings, voltage profile and lower installation cost.

Keywords: energy storage system; energy saving rate; voltage profile; installation cost; artificial neural network; improved genetic algorithm

1. Introduction

In recent years, with the rapid development of the Chinese economy, many cities are facing increasingly serious social issues, such as traffic congestion and worsening environmental pollution. For the purpose of improving the urban environment, the development of modern urban transit, which has the significant advantages of large capacity, punctuality, safety, energy conservation and environmental protection, becomes a social consensus [1,2]. Low running resistance and the use of regenerative braking are two main factors that make the metro train better than other means of transport in saving energy. In the modern urban railway system, vehicle braking energy was commonly fed back to the catenary by the method of regenerative braking. However, due to the diode rectifier of the traction supply network, surplus regenerating energy cannot feedback to a medium-voltage network. When a metro train is running in the condition of regenerative braking, if there are no adjacent accelerating trains or energy absorbing devices to absorb the regenerative energy, the train pantograph voltage would exceed the normal range, which leads to the overvoltage protection of the vehicle traction system, that is, the cancellation of regeneration braking happens [3,4]. At this moment, vehicle surplus braking energy can be only transferred into heat energy by mechanical braking or on-board resistors. Hence, how to prevent regeneration cancellation, reduce energy consumption and make full use of regenerative braking energy to improve train operation performance, have become universal concerns in world urban rail transit fields.

In order to maximize the use of the surplus energy, energy storage technologies, including the flywheel, battery and ultra-capacitor are always suggested for using in urban rail system [5–7]. Compared to other storage technology, the ultra-capacitor has the advantages of rapid charging and discharging frequencies, a long cycle life and high power density, which highly match the characteristics of urban rail transit, such as short running time between stations, frequent accelerating and braking, booming power within a short time, *etc.* Thus, the ultra-capacitor becomes a major promising alternative of energy storage technologies in the urban rail system and has gradually been applied at home and abroad [7–10]. According to the installation location of ESS, it can be divided into two kinds of installation: on-board and stationary [7]. On-board ESSs' efficiency is high with low loss in the storing and releasing of surplus energy, but restrictive in terms of vehicle weight and space; in contrast, stationary ESSs have no restrictions of weight and required space, but it is difficult to determine its best location and size, namely, the optimal place for locating and sizing, which has become an important research issue in the application of stationary ESSs. Note, there are two installation positions of stationary ESS, wayside and substation-inside. Wayside ESSs are mostly set in the track of metro line mainly for lowering the voltage fluctuation [10]. Compared to it, substation-inside ESSs are set inside TSSs (traction substations) mainly for improving the energy savings and their best location and size will be discussed in this paper.

Several literatures have involved the stationary applications for an urban rail system, mainly these concern research on energy management strategies [11–14] and optimal location and size [15–21]. In [11–14], some novel energy management strategies of stationary ESS are put forward for improving the performances of railway transit systems, and verified through experimental tests. In [15,16], the optimal design of the stationary storage device is regarded as a classical isoperimetric problem, and based on which a multi-objective optimization function is established from points of voltage fluctuation, substation current and ESS size, and then the optimized ESS size is determined by the analysis of the

energy interactive relationship between ESS and terminal substation; nevertheless, the global power flow of DC net has not been taken into account. In [17], ESSs are configured with regards to energy content, voltage variation, maximum current and power losses under different traffic conditions with an “effect-cause” simulation tool. However, the paper only analyzes the conditions with specified sizes and locations without considering other configuration possibilities. In [18], a useful method is proposed to predict the maximum instantaneous regenerative energy of each station before applying ESS and based on which the ESS configuration for each station is determined. In [19], a configuration criterion is mainly based on a polynomial approximation of the load distribution, which will be representative of the best fit for different load configurations. In [20], according to the statistic measurement of substations along Seoul metro line 2, it is summarized that substation regenerative energy is about 39% of traction energy, which offers guidance for ESS size configuration at every substation. In [21–23], a self-developed supply network load-flow software is utilized to obtain the ESS size of every substation under the constraint of DC-net voltage fluctuation and energy saving is assessed based on it.

However, through summarizing above literatures, two main configuration problems should be taken into account. First, in most literatures, ESSs are always configured based on that all substations are installed with ESS or under the condition that ESS are installed with specified sizes and locations, without considering other more optimal configuration possibilities. Second, the power levels and capacities of ESSs are generally determined by the maximum regenerative power and energy of substations in almost all literatures, but actually, some substations may present with high peak power but low mean power in certain traffic volume, under which circumstances there is no need to configure ESS with peak power. Similarly, because of the frequent energy interactive between vehicles and ESSs, smaller ESS size might be similarly suitable because of that surplus regenerative energy that cannot be absorbed would flow to adjacent ESSs.

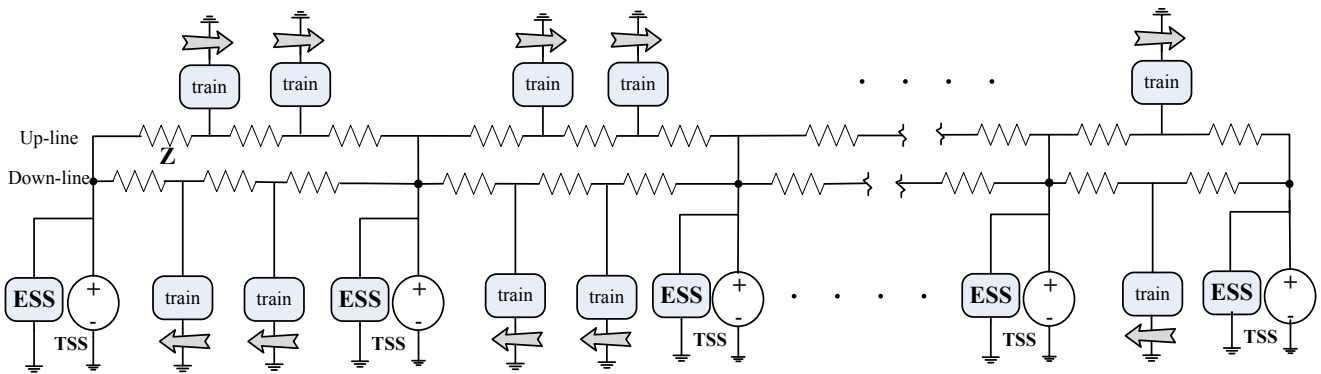
In this paper, the dynamic model of the DC rail system has been established to simulate the electrical load-flow of a traction supply network using Matlab/Simulink, and then the optimization objection is evaluated in the example of a Chinese metro line from the perspectives of energy savings, voltage profile and installation cost. Ultimately, a methodology for optimal ultra-capacitor energy storage system locating and sizing is put forward based on the improved genetic algorithm. Considering different traffic volume, the best configuration schemes can be obtained to equally satisfy the need for better energy savings, voltage profile and lower installation cost.

2. Optimizing Strategy

2.1. Background of Stationary ESS

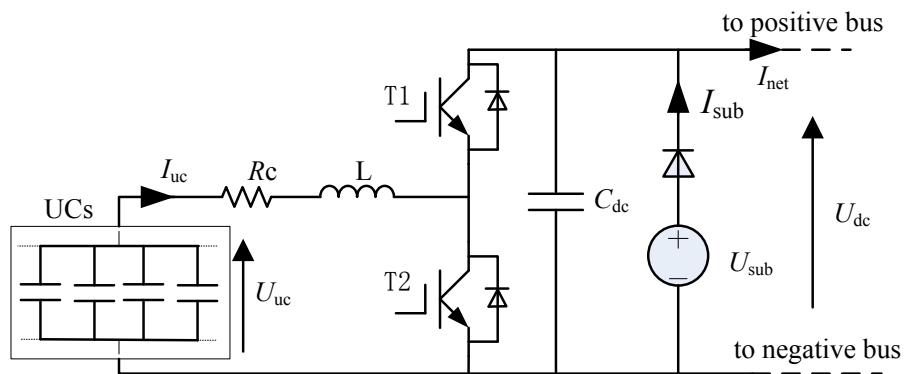
The structure of urban rail system’s DC traction power supply network is shown in Figure 1, the ultra-capacitor energy storage device is connected in parallel between the positive and negative buses of TSSs, and line impedance is expressed as Z .

Figure 1. DC traction power supply network of urban rail system.



An energy storage device consists of a bidirectional DC/DC converter and UCs (ultra-capacitors), and its charging and discharging process are controlled by the switch tubes T1 and T2, as shown in Figure 2. Ultra-capacitor modules are coupled by the bidirectional dc-dc converter with the TSS and dc electric network. Where I_{uc} is the current that flows into the UC modules; U_{uc} is the terminal voltage of UCs; U_{sub} and I_{subr} are respectively the terminal voltage and the output current of rectifier units of TSS; U_{dc} is DC bus voltage; I_{net} is the current that flows into dc network. When ultra-capacitors are in the charging state, substation rectifier units quit operation, and there is no current flow from substation in the meantime.

Figure 2. UCs coupled by the bidirectional DC/DC converter with TSS.



2.2. Optimizing Strategy

2.2.1. Objective Function

In this paper, the objective of the optimal for ESS locating and sizing is to obtain the best energy savings and voltage profile with the minimum installation cost. Therefore, the paper put forward the following objective functions.

a. Energy saving rate, E_{rate}

Take the sum of output energy consumption of all TSSs along the metro line in a single vehicles time span as the traction energy consumption:

$$W_{sub} = \sum_1^k \left[\int_0^T (I_{sub} \cdot U_{sub}) dt \right] \tag{1}$$

where k is the number of traction substations; T is the single vehicles time span.

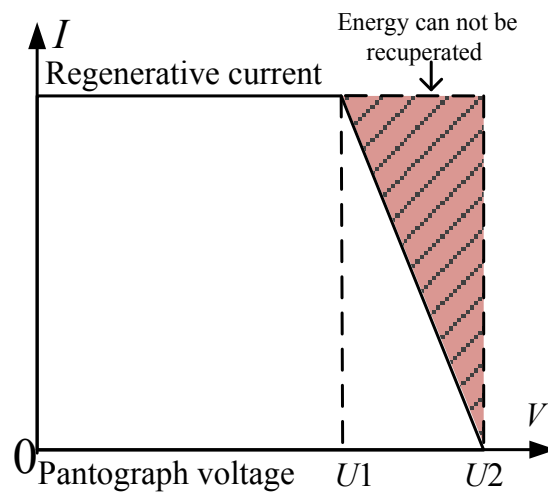
Energy saving rate is given as a percentage of the difference among the maximum traction energy consumption without and with ESSs.

$$E_{rate} = \left(1 - \frac{W_{sub}^{uc}}{W_{sub}^{nouc}} \right) \times 100 \tag{2}$$

b. Regeneration cancellation rate, V_{rate}

When the urban rail train is running under the condition of regenerative braking, its ideal regenerative current limit curve is shown in Figure 3. If its pantograph voltage exceeds $U1$, partial regeneration cancellation will happen, the regenerative current will wane to reduce the feedback energy from regenerative braking, and the reductive braking force will be complemented by the mechanical braking force. When the pantograph voltage exceeds $U2$, the regenerative braking operation will cease completely, and the braking force will be totally supplied by mechanical braking.

Figure 3. Ideal regenerative current limit curve of urban rail train.



Ultra-capacitors can inhibit the rise of train pantograph voltage and reduce the probability of regenerative braking cancellation; thus, this paper takes the regeneration cancellation rate V_{rate} to evaluate the voltage profile after the installation of ESSs.

$$V_{rate} = \frac{\sum_1^n T_{(V>U1)}}{\sum_1^n T_{line}} \cdot 100 \tag{3}$$

where T_{line} is the train operation period; $T_{(V \geq U1)}$ is the summational time when regeneration cancellation happens; n is the amount of up-line and down-line trains.

c. Installation cost, C

An ultra-capacitor energy storage device is composed of a control device (dc-dc converter, inductor, reactor, etc.) and ultra-capacitors; thus, the installation cost of ESSs along urban rail line can be calculated as the following formula:

$$C = P_{uc} \times M_{con} + E_{uc} \times M_{uc} \tag{4}$$

where, P_{uc} is the total power level of control device; M_{con} is the cost of control device per MW; E_{uc} is the total energy storage capacities of ESSs along whole line; M_{uc} is the ultra-capacitor cost per kWh.

d. Objective function, $ObjV$

Given the energy saving, voltage profile and economy of ESS, the objective function of optimal energy storage for locating and sizing is shown as below:

$$ObjV = \omega_1 \cdot \frac{E_{ratemax} - E_{rate}}{E_{ratemax}} + \omega_2 \cdot \frac{V_{rate} - V_{ratemin}}{V_{ratemax} - V_{ratemin}} + \omega_3 \cdot \frac{C}{C_{max}} \tag{5}$$

where $E_{ratemax}$ is the maximum value of E_{max} ; $V_{ratemax}$ and $V_{ratemin}$ are respectively the maximum and minimum of V_{rate} ; $E_{ratemax}$ and $V_{ratemin}$ can be obtained when all TSSs are installed with ESSs of infinite size; meanwhile, C_{max} can be calculated basing on their corresponding available ESSs capacities and powers; $V_{ratemin}$ can be obtained when there are no ESSs installed along total metro line. It is worth noting that the value of $E_{ratemax}$, $V_{ratemax}$, $V_{ratemin}$ and C_{max} are different under different traffic conditions. ω_1 , ω_2 , ω_3 are respectively the weight coefficients of E_{rate} , V_{rate} and C after the process of normalization and they represent the emphasis degrees of energy saving, voltage profile and installation cost from the subway operator.

2.2.2. Constraint Condition

a. Substation voltage/current constraint:

$$\begin{cases} 600 \leq U_{sub}^{(k)} \leq 900 \\ I_{sub}^{(k)} \geq 0 \end{cases} \tag{6}$$

b. SOC constraint:

SOC(State of Charge) of ultra-capacitor is defined as follow:

$$0.25 \leq SOC = \frac{E_{uc}}{E_{ucmax}} = \frac{0.5CU_{uc}^2}{0.5CU_{ucmax}^2} = \left(\frac{U_{uc}}{U_{ucmax}} \right)^2 \leq 1 \tag{7}$$

The storage energy of ESS is proportional to the square of terminal voltage. When the ultra-capacitor is in the state of charging, the terminal voltage changes significantly. When ultra-capacitors are in the state of discharging, a low terminal voltage will lead to a difficult boost function of the DC/DC converter; thus, the terminal voltage of ultra-capacitors is generally set between $0.5U_{ucmax}$ and U_{ucmax} , that is, the range of SOC varies from 0.25 to 1.

c. Charging and discharging constraint:

$$\begin{cases} \int_0^T U_{uc} I_{uc} dt = 0 \\ |U_{uc} I_{uc}|_{\max} \leq P_{level} \end{cases} \quad (8)$$

In order to ensure that the ESS has enough free storage space to absorb surplus regenerative energy of the DC supply network, the charging and discharging energy of ESS should finally reach consensus in single vehicle time span. Meanwhile, the maximum of charging and discharging power must be below the configured power level.

In conclusion, the optimal locating and sizing of ESSs is to solve minimum of $ObjV$ in premise of above constraint conditions.

3. Simulation Methodology

3.1. Case Study

To assess the reasonability of optimization strategy, a sample urban railway line is studied in this paper. The total length of the line is about 24.6 km along with 22 stations, of which there are 13 traction substations and their distribution is shown in Table 1. The vehicle data and DC network parameters are shown as Table 2. These parameters are provided by Beijing Subway Company.

Table 1. TSS spacing distances.

No.	1	2	3	4	5	6	7	8	9	10	11	12
Spacing(km)	1.11	1.93	2.16	2.3	2.12	2.7	2.76	1.53	1.77	1.88	2.6	1.0

Table 2. Vehicle data.

Parameter	Value	Parameter	Value
Formation	3M3T	Inverter efficiency	0.97
Load Condition	312.9t (AW3)	Motor efficiency	0.915
Rated voltage	750 V	Gearing efficiency	0.93
AC motor/M	180 kW × 4	Max speed	80 km/h
SIV Power	160 kVA × 2	Maxacceleration	1 m/s ²
SIV Power factor	0.85	Min deceleration	−1 m/s ²
Floating Voltage U_s	836 V	Equivalent internal resistance R_s	0.07 Ω
Contract line impedance	0.007 Ω/km	Rail impedance	0.009 Ω/km
Pantograph impedance R_f	0.015 Ω	—	—

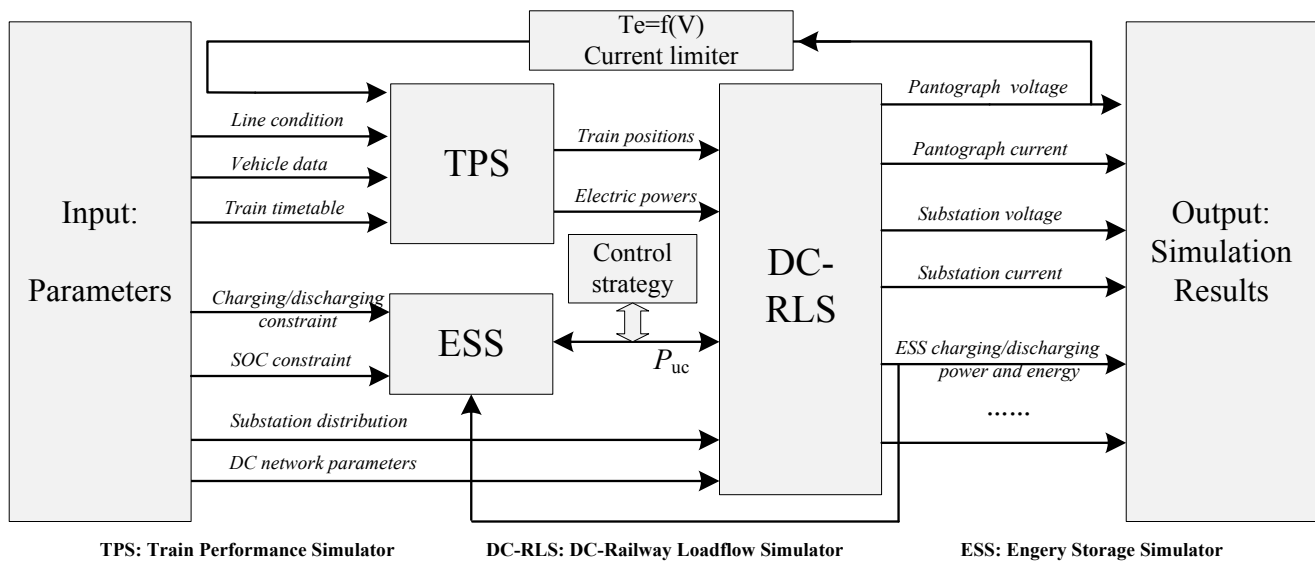
The ESSs are installed in every traction substation. According to the simulation experience, the maximum of ESSs peak power are lower than 2 MW, and their capacities are always less than 10 kWh. Thus, the initialization values of the ESS size are 2 MW/10 kWh, and the charging and discharging thresholds of ESS are respectively 850 V and 800 V.

According to the analysis of the train timetable, the sample case will be simulated respectively under three major traffic scenarios: low traffic volume with vehicles time span of 600 s, moderate traffic volume of 300 s and high traffic volume of 150 s. This will be done with the following simulation platform.

3.2. Simulation Platform

For the goal to simulate the power flow of the DC network of an urban rail system, the simulation platform of the DC railway is established in the Matlab environment, as shown in Figure 4. The platform includes a train performance simulator (TPS), a DC railway load-flow simulator (DC-RLS) and an ultra-capacitor energy storage system (ESS). By neglecting the fast transients of trains' state change in single simulation step size, the DC supply network can be described as a sequence of stationary states whose input data are total urban rail trains' electric powers and their corresponding present positions.

Figure 4. Simulator for ultra-capacitor energy storage system.



TPS:

As shown in Figure 4, the output of TPS is not only associated with line condition, vehicle data and timetable, but is also constrained by real-time train pantograph voltage. From TPS we can get positions of up-line and down-line trains and their corresponding electric power, which offer essential data for subsequent load-flow calculation of the DC supply network.

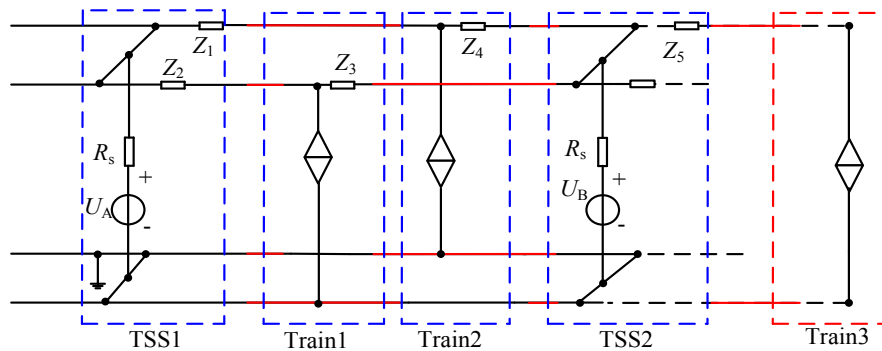
DC-RLS:

In the solving process of the DC electric network, because of its time-variation (network topology change with train movement) and nonlinearity (nonlinearity of substation and regenerative braking) of the network structure, the paper presents a new load-flow calculation methodology of component segmentation: the simulation result demonstrates the rapidity and astringency of this methodology which will be shown as follows.

(1) Component segmentation

As shown in Figure 5, the DC electric network can be segmented into two types of components, TSS and train. In this figure, there are only two trains running between TSS1 and TSS2. However, it is worth noting that the number of trains between two TSSs would increase to three or four in high traffic volume by analysis of the timetable.

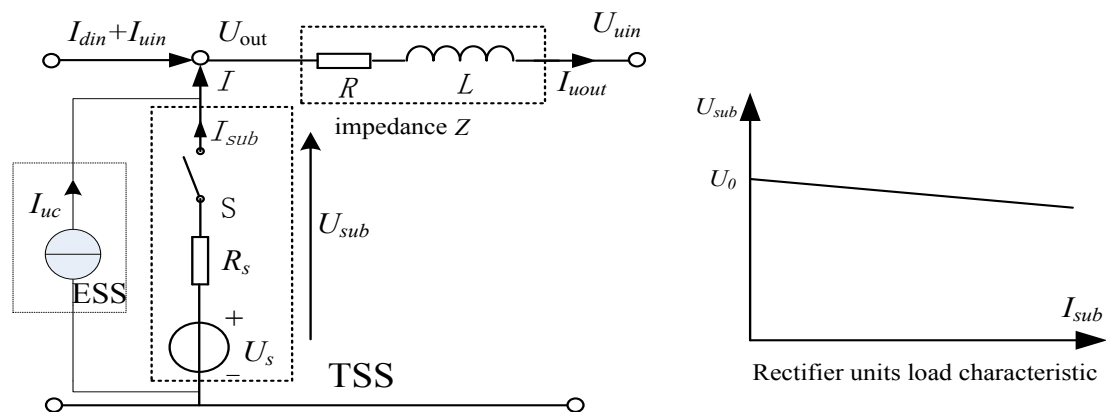
Figure 5. Segmentation of DC electric network.



(2) Subsystem component

The TSS component consists of substation and its right connected impedance Z , which is determined by the distance to next adjacent component. The ideal voltage source U_s and its equivalent internal resistance R_s are series connected to simulate the rectifier units load characteristic. Because of the no-controlled diode rectifying mode of TSS, the substation output current flows unidirectionally. As shown in Figure 6, when substation output current I_{sub} is positive, switch S close; when I_{sub} is negative, S break. U_0 is substation no-load voltage. ESS is equivalent to the controlled current source and be controlled by energy control strategy which will be introduced in the following.

Figure 6. TSS component.



$$\frac{dI}{dt} = \frac{1}{L} ((U_s - U_{uin}) - R(I_{uin} + I_{din} + I) - R_s I - L \frac{d(I_{din} + I_{uin})}{dt}) \tag{9}$$

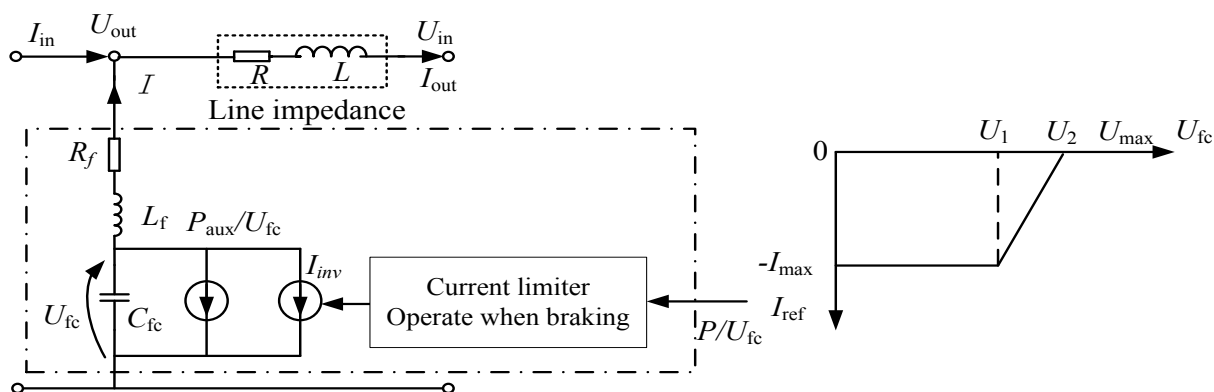
$$U_{out} = U_{uin} + R I_{uout} + L \frac{dI_{uout}}{dt} \tag{10}$$

$$I_{uout} = I_{uin} + I_{din} + I \tag{11}$$

$$I = I_{uc} + I_{sub} \tag{12}$$

As shown in Figure 7, the train component consists of the vehicle and its right connected impedance Z which is determined by the distance to next adjacent component; R_f is vehicle filter resistance; L_f is vehicle filter inductance, C_{fc} is vehicle support capacitor; P_{aux} is auxiliary power; P is vehicle electric power.

Figure 7. Train component.



$$\frac{dI}{dt} = \frac{1}{L + L_f} ((U_{fc} - U_{in}) - R(I + I_{in}) - R_f I - L \frac{I_{in}}{dt}) \tag{13}$$

$$\frac{dU_{fc}}{dt} = \frac{1}{C_f} (-I - I_{inv} - P_{aux} / U_{fc}) \tag{14}$$

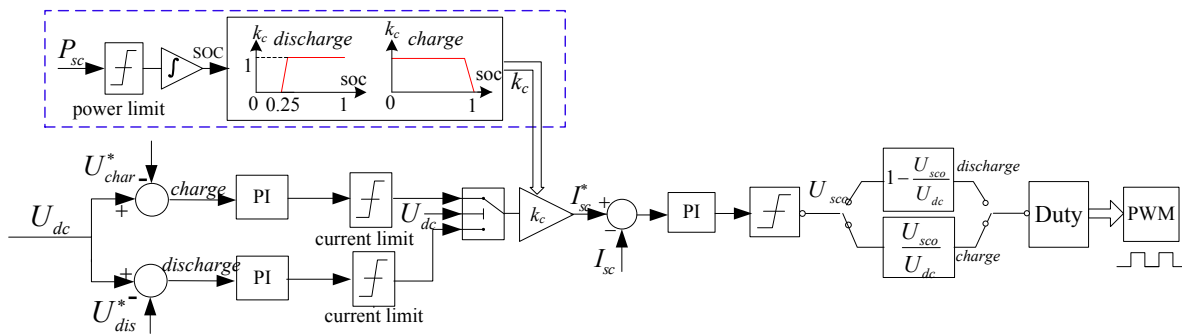
$$U_{out} = U_{in} + R I_{out} + L \frac{dI_{out}}{dt} \tag{15}$$

$$I_{out} = I_{in} + I \tag{16}$$

ESS:

The energy control strategy of stationary ESS can be divided into three parts: DC network voltage constraint, charging/discharging control, and SOC constraint. U_{char} and U_{dis} are respectively the threshold values of charging and discharging, the magnitude and direction of charging and discharging current are determined by the difference value between current voltage and threshold value. When the DC network voltage fluctuates between U_{dis} and U_{char} , ultra-capacitors maintain the standby state. The working range of SOC is 0.25~1 for the restriction of charging and discharging the current of ultra-capacitors. The control strategy is shown in Figure 8.

Figure 8. Stationary ESS energy control strategy.



3.3. Simulation Output

Figure 9 shows where the speed and electric power of up-line train are exported from TPS. Figure 10 shows where the up-line train pantograph voltage and current are. When up-line train is braking, the pantograph voltage may exceed 900 V, which results in regenerative braking cancellation. Take TSS2 for example, its terminal voltage and net current under low traffic volume are shown in Figure 11, and it can be observed that the voltage and current fluctuate periodically with the time span of 600 s. The charging/discharging power and its SOC waveform of ESS that installed in TSS2 are shown in Figure 12, when its power is positive, ESS maintains the charging state with an increasing SOC value. On the contrary, ESS is in the discharging state with decreasing SOC value: SOC varies between 0.25 and 1.

Figure 9. The speed and electric power of up-line train.

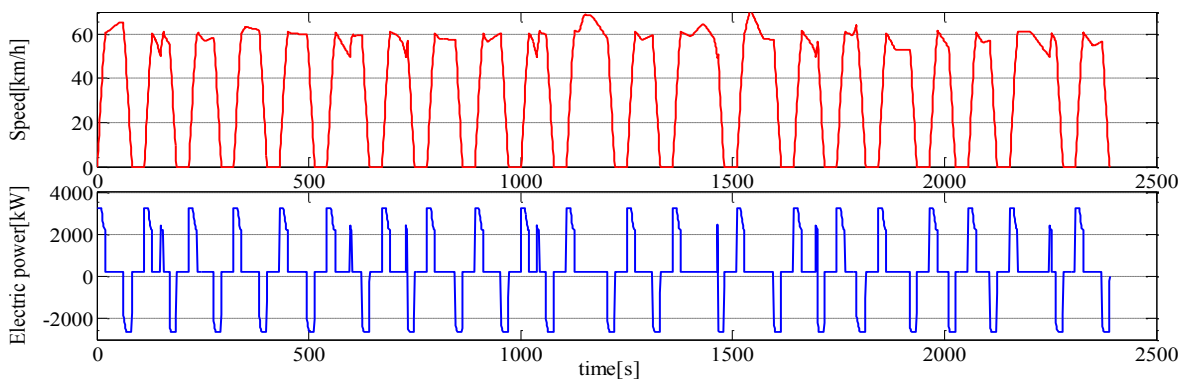


Figure 10. The pantograph voltage and current of up-line train.

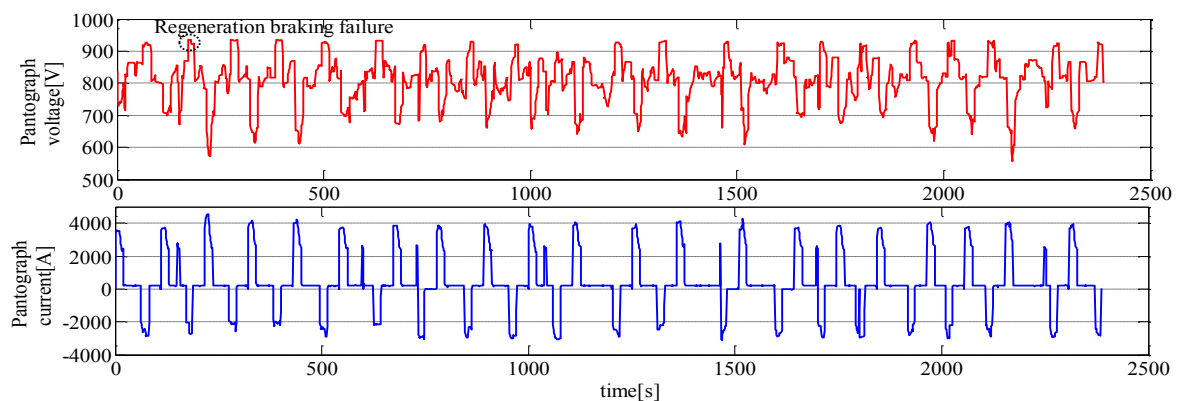


Figure 11. TSS terminal voltage and net current.

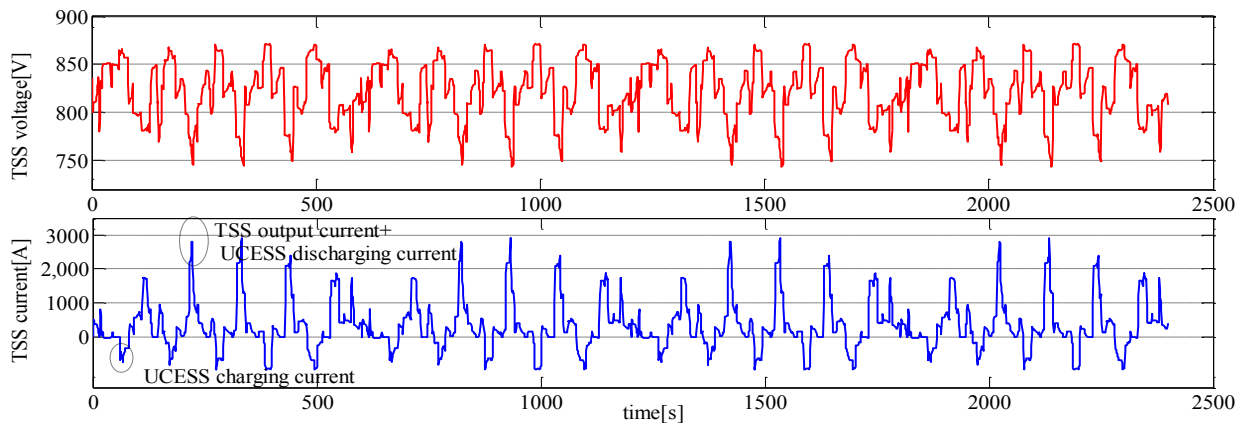
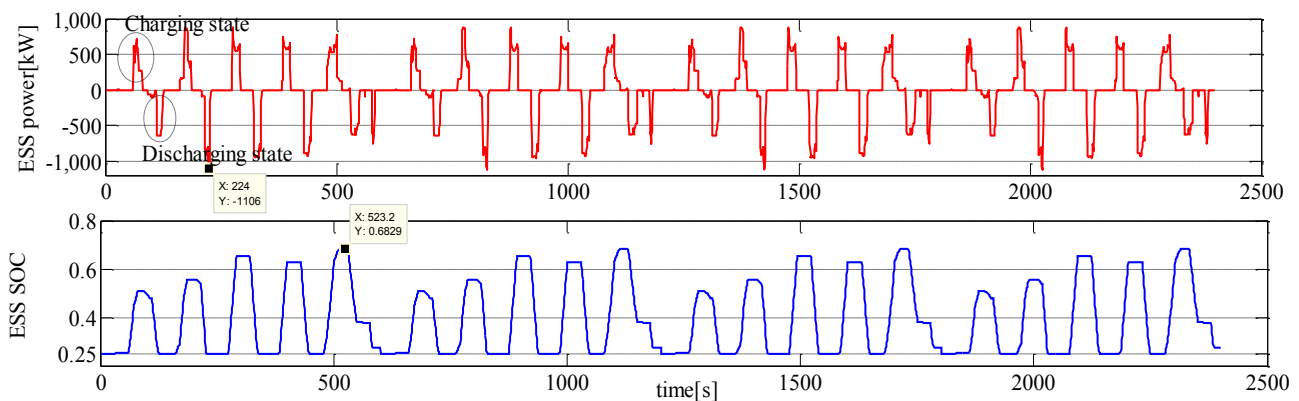


Figure 12. ESS charging/discharging power and SOC.



In a traditional configuration method, the capacities of ESSs can be calculated based on the maximum of SOC by Formula (17).

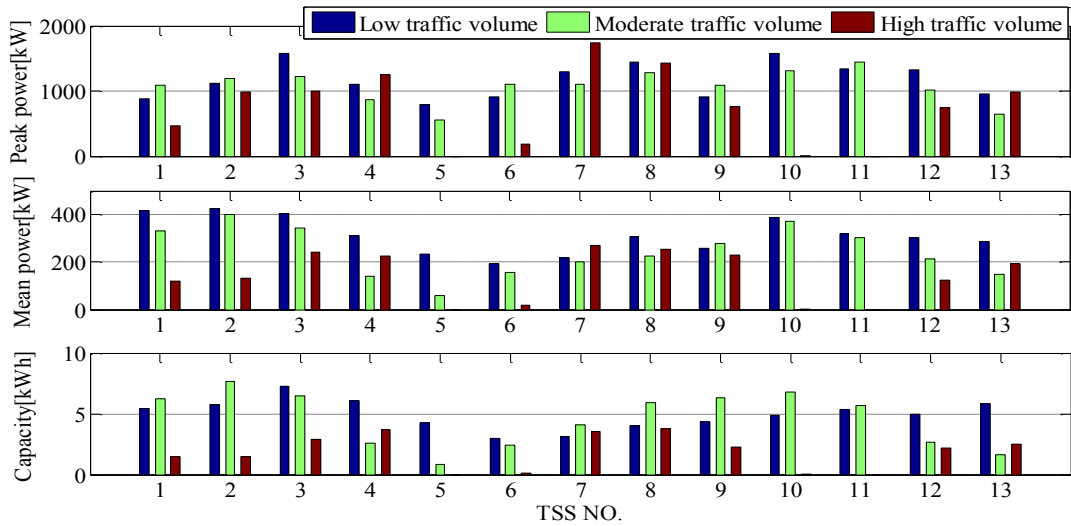
$$E_{actual} = E_{initial} * (SOC_{max} - 0.25) / 0.75 \tag{17}$$

The power levels of ESSs are determined by the maximum charging or discharging power. Take TSS2 for example, its initial ESS capacity is set at 10 kWh; therefore, we can calculate that its capacity of ESS is 5.42 kWh, and its peak power is 1.1 MW from Figure 12. The statistic values of peak and mean power, and the capacity of each substation’s ultra-capacitors under different traffic volume are shown in Figure 13.

From Figure 13, it is observed that the powers and capacities of ESSs under low and moderate traffic volumes are similar, but are much greater than that when there is high traffic volume.

With the decreasing of the vehicle’s time span, the probability of simultaneous regenerative braking in two or more trains increases, and the frequency of energy interaction between trains increases, too. In high traffic volume, the effect of energy interaction plays a greater and more important role, which leads to much less surplus regenerative energy being stored in the DC supply network. The high train density might also result in high instantaneous peak power derived from multi-trains’ simultaneous braking, as shown in TSS7 whose peak power is nearly 1.70 MW but mean power is only 271 kW in high traffic volume.

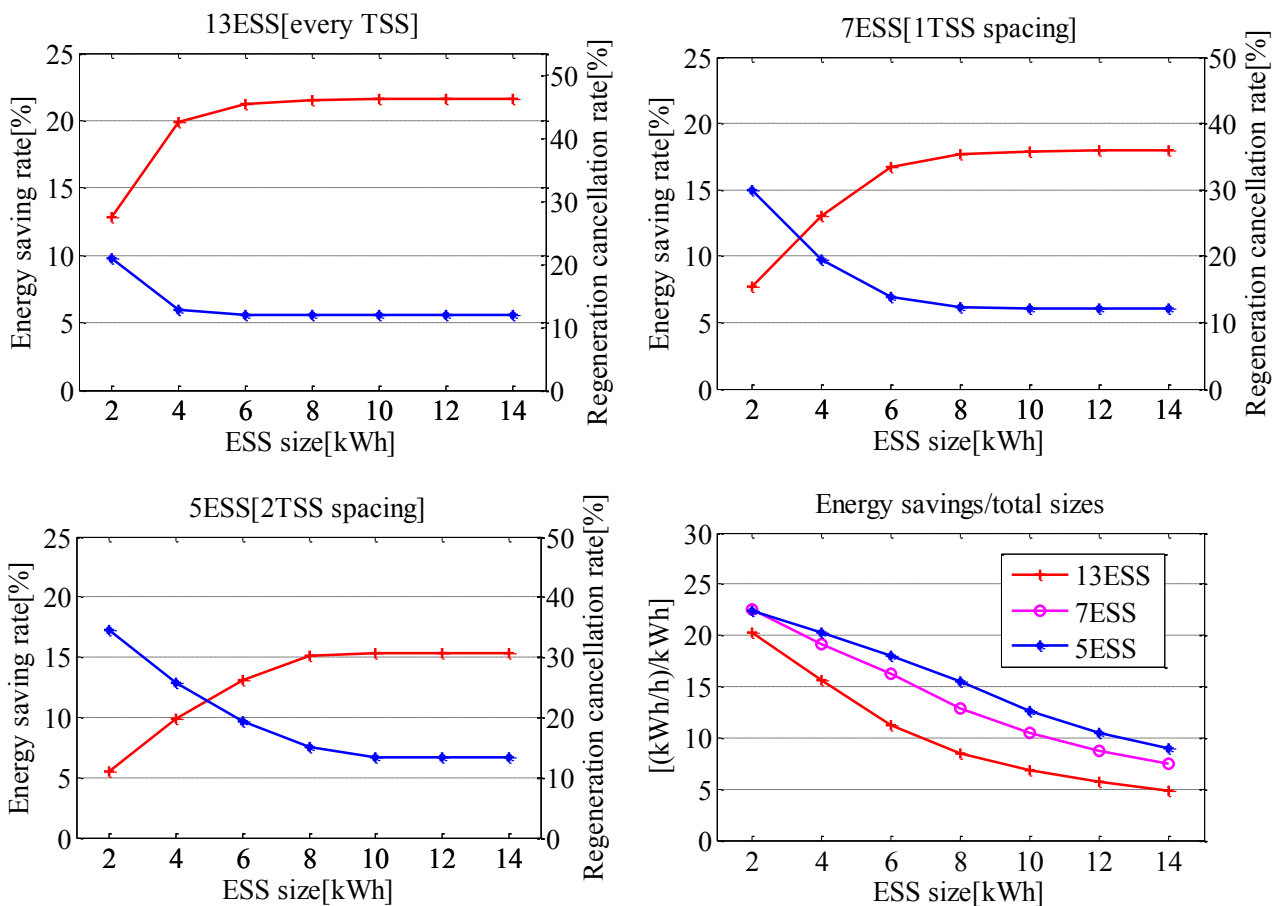
Figure 13. ESS power and capacity of every TSS.



3.3. Location and Size Assessment

The main goal of above simulations is to evaluate the energy saving and voltage profile in the metro line by using stationary ESS and to help finding the best location and size. Thus, ESS distributions every TSS, 1TSS spacing, 2TSS spacing for the seven proposed sizes (2, 4, 6, 8, 10, 12 and 14 kWh) will be simulated under low traffic volume. Simulation results are shown in Figure 14.

Figure 14. Energy saving rate and regeneration cancellation rate diagram.



The energy saving rate and regeneration cancellation rate of the above three distribution schemes are compared in the above figures. Obviously, when all TSSs are set with ESS, the energy saving rate goes up to the maximum value of 21.64% and the regeneration cancellation rate reduces to the minimum value of 11.88%. As the number of ESSs decreases, the energy saving rate presents a declining trend and the regeneration cancellation rate displays a rising trend. Under the same distribution scheme, with the increase of ESS size, the energy saving rate increased sharply and then slowed down to a constant value, while the regeneration cancellation rate decreases and the latter flattens.

In the charging process, ESS absorbs the surplus regenerative energy of the DC-net in order to avoid the accumulation of surplus energy, which may lead to regenerative braking cancellation; namely, ESSs lower the regeneration cancellation rate. In the discharging process, ESSs provide energy for adjacent trains powering operation, which decrease the output energy consumption of substations, and increases the energy saving rate. Therefore, under the constraint condition that the charging and discharging energy of ESS finally reach consensus, energy saving rate is negatively correlated to regenerative cancellation rate, which is consistent with the simulation results.

To evaluate the global performance of the system, the concept of energy saved per ESS size installed in the line is introduced in the bottom right corner graph of Figure 14. The tendency is clear that the ESS performance decreases with the size installed. However, it is noticed that the global energy saving rate increases with this parameter. A compromise between these two values should be found, namely, a high energy saving rate with acceptable ESS performance.

Because of their inverse relationship between energy saving rate and regeneration cancellation rate, the objective function can be further simplified by setting the weight coefficient of regeneration cancellation rate ω_2 equal 0, thus the final objective function would be described with energy saving rate, installation cost and their corresponding weights. The regeneration cancellation rate will be reserved for later analysis.

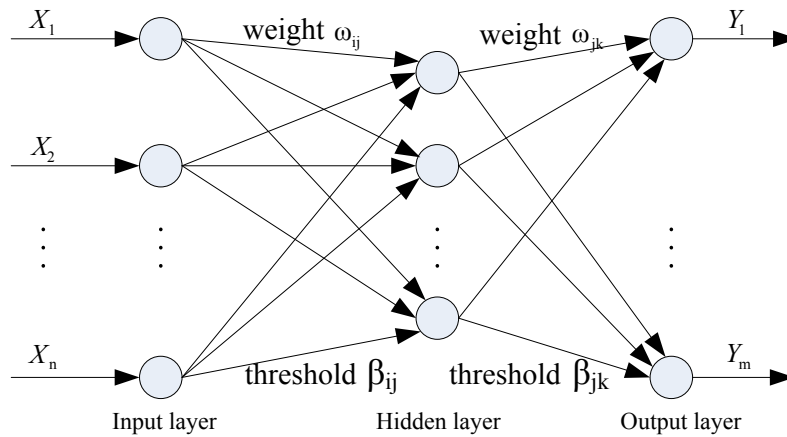
4. Optimal Locating and Sizing

4.1. BP Neural Network

In the solving process of the DC electric network using a simulation platform, because of the time-variation and nonlinearity of the network structure, the solving speed is affected greatly by the presence of high simulation precision. In order to improve subsequent optimization efficiency, the paper utilizes BP artificial neural network (BP-ANN) to fit the actual DC electric network [24,25].

BP-ANN topological structure is shown as Figure 15, where X_1, X_2, \dots, X_n are the inputs of BP-ANN; and Y_1, Y_2, \dots, Y_m are the forecast values. There are n input nodes and m output nodes, that is, BP-ANN expresses the mapping relation from n independent variables to m dependent variables. In the paper, n represents the size (capacity and power level) of ESSs installed in 13 TSSs, and m is the energy saving rate and regeneration cancellation rate.

Figure 15. BP-ANN topological structure diagram.

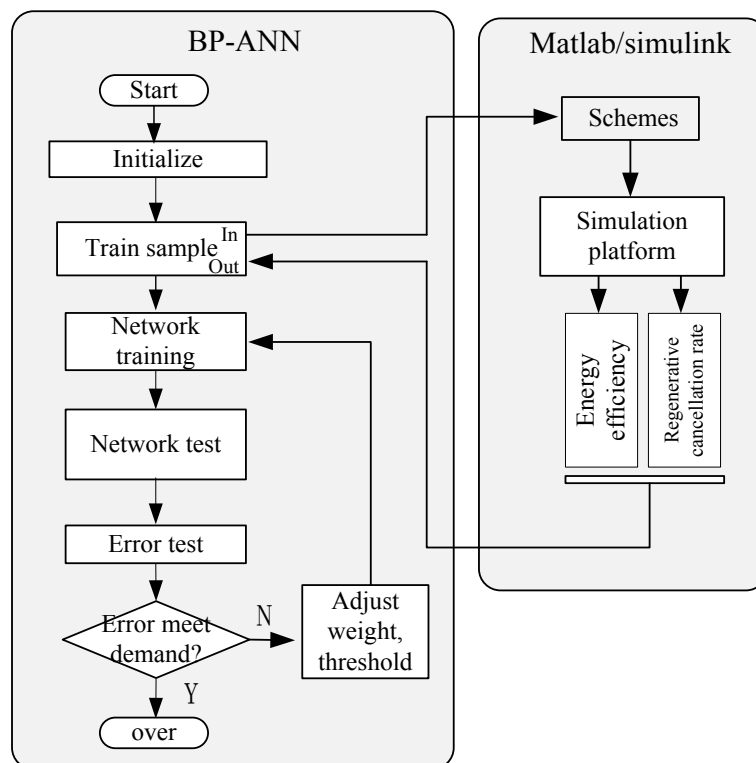


The forecast values of BP-ANN are closer and closer to the expected output by training the weights and thresholds of BP-ANN in the basis of forecast error E :

$$\begin{cases} \omega_{ij}(t+1) = -\eta \frac{\partial E}{\partial \omega_{ij}} + \omega_{ij}(t), \omega_{jk}(t+1) = -\eta \frac{\partial E}{\partial \omega_{jk}} + \omega_{jk}(t) \\ \beta_{ij}(t+1) = -\eta \frac{\partial E}{\partial \beta_{ij}} + \beta_{ij}(t), \beta_{jk}(t+1) = -\eta \frac{\partial E}{\partial \beta_{jk}} + \beta_{jk}(t) \end{cases} \quad (18)$$

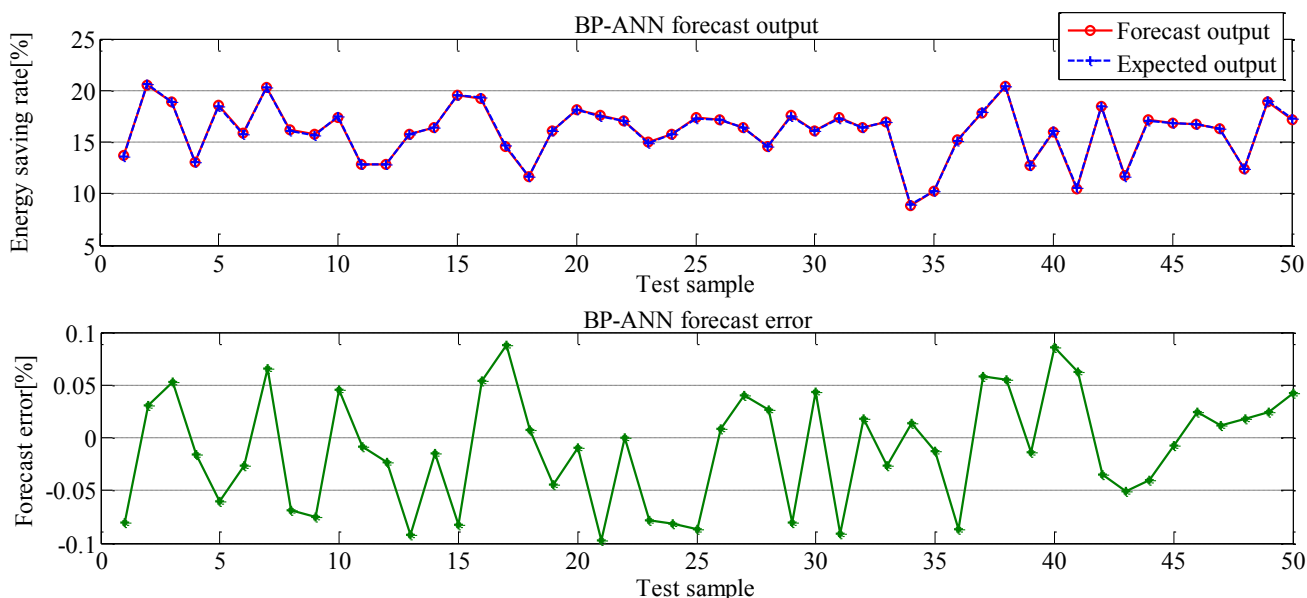
Take low traffic volume for example, the paper gets 5000 input-output samples based on the simulation platform, select 4950 samples as network training samples, and the remaining 50 samples as network test samples. The BP-ANN structure is 13-7-2; the network training flow chart is shown in Figure 16.

Figure16. BP-ANN flow chart.



As shown in Figure 17, where are the comparisons between the energy saving rates forecasted by trained BP-ANN and their corresponding desired outputs. It points out that the trained BP-ANN has a high fitting degree whose forecast errors between forecast outputs and expected outputs are less than $\pm 0.1\%$, and the single solution time decreases from the minute level by simulation platform to the millisecond level by BP-ANN.

Figure 17. BP-ANN expected outputs and errors.



4.2. Genetic-Annealing Algorithm

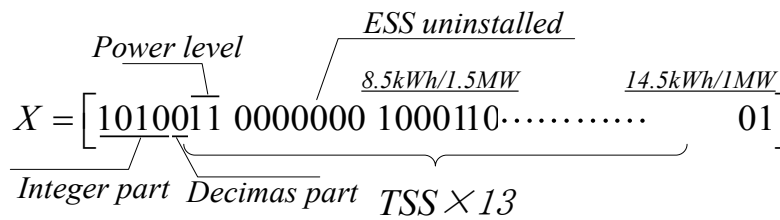
4.2.1. Genetic Algorithm

The genetic algorithm (GA) is a global optimal searching algorithm based on Darwin’s nature evolution theory and Mendel’s genetics and mutation theory. It consists of three parts: encoding, fitness evaluation and genetic manipulation [26–28]. Combined with paper demands, the basic procedures of the genetic algorithm are shown as follows.

(1) Encoding

The location and size of ESSs installed in 13 TSSs can be encoded by 13×7 binary numbers as shown in Figure 18, where each X chromosome represents a population individual, the ESS capacity in every TSS is shown with five binary numbers, whose previous four numbers represent the integer portion of size, and the last number represents the decimal part of size. The ESS power level in every TSS is shown with two binary numbers; 00, 01, 10 and 11 respectively represent 0.5 MW, 1 MW, 1.5 MW and 2 MW. If the capacity of one TSS is all 0, it means that ESS is uninstalled in this TSS. The initialization population number is NIND, and the length of population individual is PRECI.

Figure 18. The encoding structure of ESSs location and size.



(2) Fitness evaluation

In this paper, the optimal locating and sizing of ESSs is to solve the minimum of *ObjV*, thus, the reciprocal of *ObjV* is calculated as the fitness value. The fitness formula is shown as follows:

$$\begin{cases} ObjV[X] = \omega \cdot \frac{E_{rate\max} - ANN(X)}{E_{rate\max}} + (1 - \omega) \cdot \frac{C(X)}{C_{\max}} \\ Fitness[X] = \frac{1}{ObjV[X]} \end{cases} \quad (19)$$

where *ANN(X)* is the energy saving rate simulated from BP-ANN with the input of *X*; *Fitness[X]* is the fitness value of *X*.

(3) Genetic manipulation

Genetic manipulation includes three basic steps—selection, crossover and mutation—which is consistent with the traditional procedures; thus, no detailed introduction will be made about genetic manipulation in this paper.

Compared with other intelligence algorithms, genetic algorithm has a higher rate of convergence, more efficient calculation and higher robustness. However, in this paper, optimization results tend to converge to local optimal solutions rather than global optimal solutions with typical GA, and premature phenomena occur. Thus, a hybrid algorithm is offered that combined genetic algorithm and simulated annealing algorithm to solve the problem of premature phenomena.

4.2.2. Simulated Annealing

The simulated annealing (SA) algorithm takes the physical image and statistical properties of solid annealing process as physical background, and generally uses a metropolis criterion to decrease the probability of local convergence [29–31]. On the basis of the above typical genetic algorithm, the following steps are added to typical GA:

(1) Difference between objective function values:

New solution *X_j* is obtained from the genetic operation based on current solution *X_i*, and then calculates the corresponding objective function values *ObjV(X_i)*, *ObjV(X_j)*. The difference between objective function values:

$$\Delta\Phi = ObjV(X_j) - ObjV(X_i) \quad (20)$$

(2) Metropolis criterion

Metropolis acceptance probability is the probability to be accepted of X_j :

$$P = \begin{cases} 1, & \Delta\Phi < 0 \\ \exp(-\Delta\Phi / T), & \Delta\Phi > 0 \end{cases} \quad (21)$$

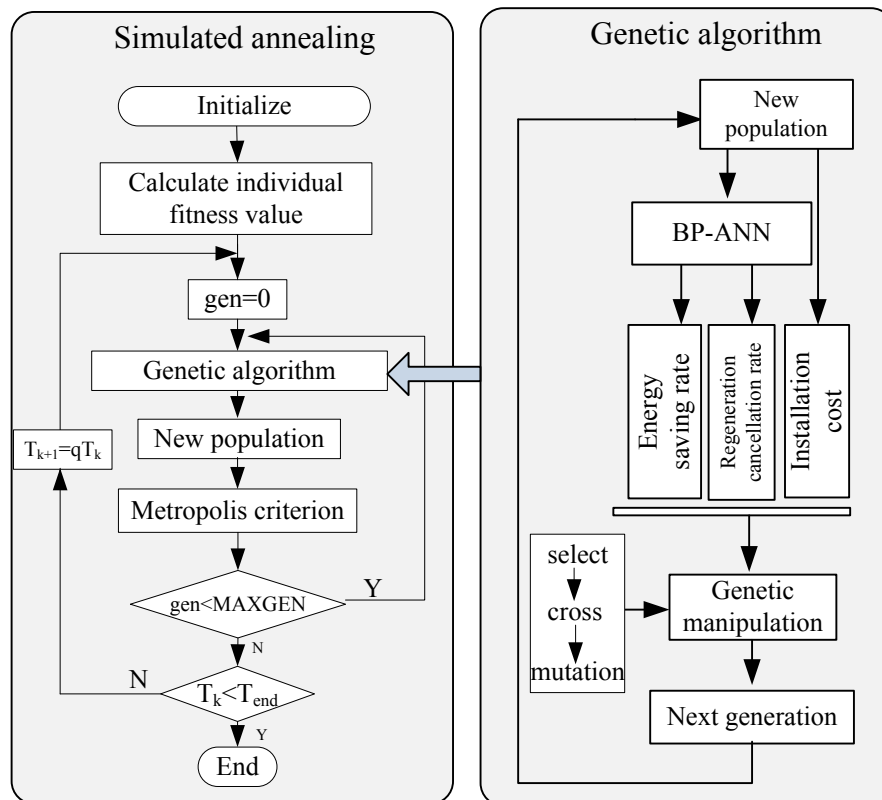
$$T_{k+1} = T_k * q \quad (22)$$

where T is the current temperature of the annealing process, which decreases as time goes by; q is temperature decreasing coefficient, $0 \leq q \leq 1$; k is the iterations of annealing process.

4.2.3. Genetic-Annealing Algorithm

In the early period of the GA process, the stretch effect of SA for GA fitness is not strong, the probabilities of offspring from individuals with close fitness are similar; when temperature T is decreasing in the later period of GA process, the stretch effect strengthens, and the difference between individuals with close fitness increases, which makes the advantage of a superior individual more obvious, and sequentially avoids the problem of local convergence. The SAGA flow chart is shown as Figure 19.

Figure 19. SAGA flow chart.



The relevant parameters of SAGA are given by Table 3, the crossover rate of GA is P_c , and the mutation rate is P_m . M_{con} is 0.32 which means that the cost of ESS control segment is 0.32 million dollars per MW, M_{edlc} is 0.04 which means that the cost of ultra-capacitors is 0.04 million dollars

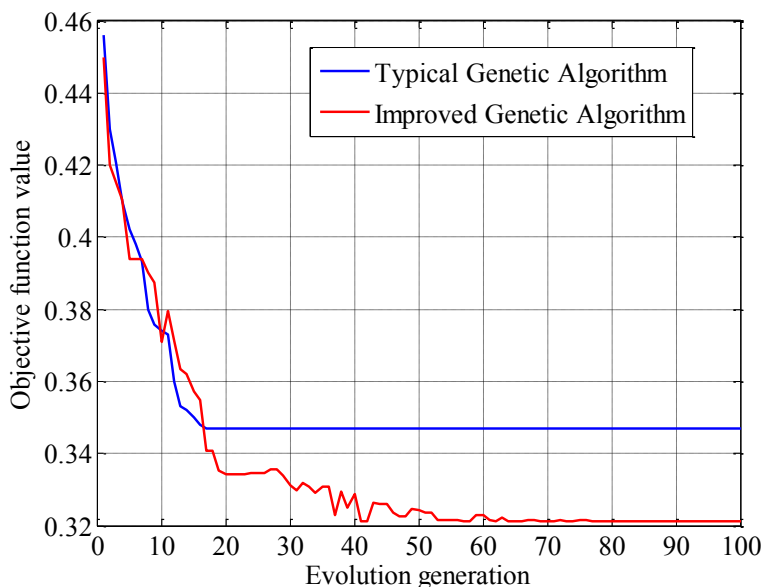
per kWh, M\$/kWh. The values of M_{con} and M_{edlc} are only the reference values of this paper rather than the actual values in an engineering application.

Table 3. SAGA parameters.

<i>NIND</i>	<i>PRECI</i>	P_c	P_m	T_0
100	91	0.8	0.015	100 °C
T_{end}	q	<i>MAXGEN</i>	M_{con}	M_{edlc}
1 °C	0.8	10	0.32	0.04

The evolution curve of optimization process for ESS locating and sizing is shown in Figure 20. When optimized only with typical GA in low traffic volume where ω equals 0.5, the evolution curve converges to a local optimal solution with an objective function value of 0.347. After the addition of SA, the curve declines in the form of oscillation. When evolution generation increases to 80, the curve convergence to the global optimal solution with the objective function value of 0.321, the minimum of *ObjV* is obtained and its corresponding solution is the optimization result for ESS locating and sizing.

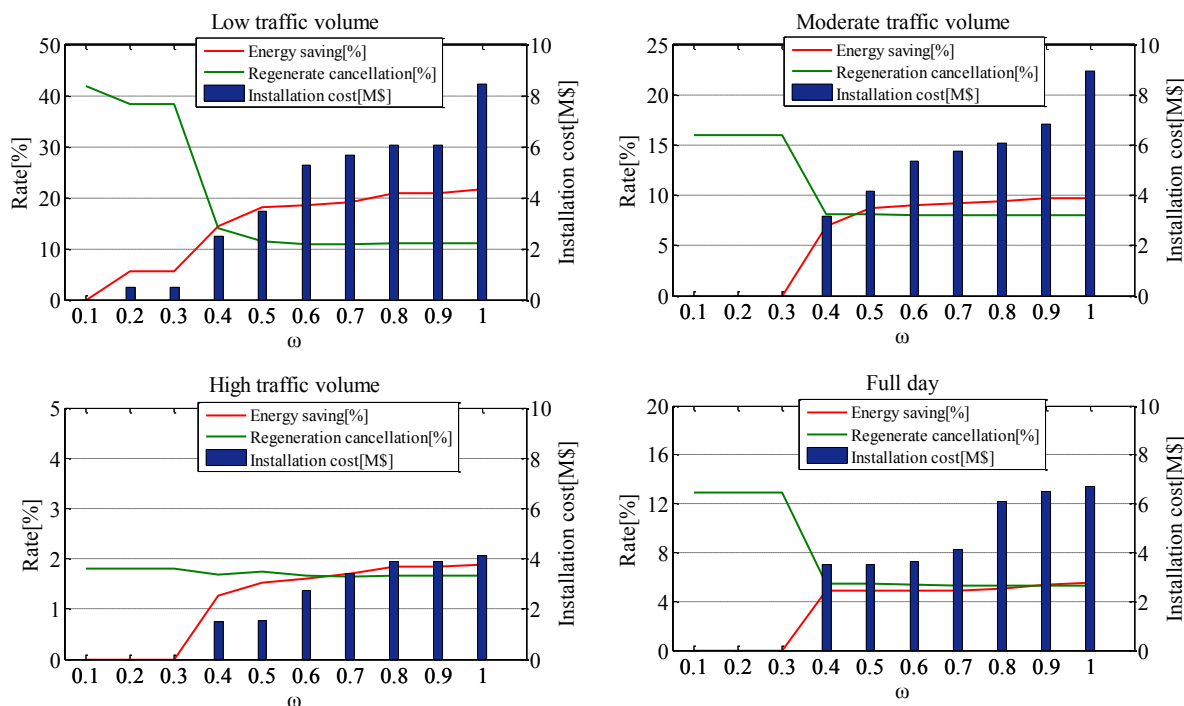
Figure 20. Comparison of the evolution curve.



4.3. Optimization Result Analysis

The best ESSs locating and sizing schemes under different traffic conditions can be obtained by SAGA with a different weight coefficient of the energy saving rate ω , as shown in Figure 21. It is worth noting that the conventional schemes are obtained based on the traditional configuration method and is shown with ω to be 1. The optimization schemes are shown when ω changes from 0.9 to 0.1.

Figure 21. Optimized results under different traffic volumes.



4.3.1. Low Traffic Volumes

As seen in first graph of Figure 21, in the conventional scheme ($\omega = 1$), the best energy saving rate (21.64%) and regeneration cancellation rate (11.88%) can be obtained with an installation cost of 8.62 M\$. With a decrease of ω , obviously, the energy saving rate and regeneration cancellation rate become worse with a coinciding decrease in installation cost. When ω is 0.9, the energy saving rate and regeneration cancellation rate change little compared to the conventional scheme, but the installation cost declines from 8.62 M\$ to 6.06 M\$, and the number of TSSs set with ESSs decreases to 10. When ω decreases to 0.5, the energy saving rate decreases to 18.01%, the regeneration cancellation rate rises to 14.40%, but the installation cost experiences a large decline to 3.48 M\$ with only six TSSs set with ESSs. It can be observed that the improved genetic algorithm has a good optimization function on the location and size of ESSs, and the impact degree of energy-saving and installation cost are decided by the weight coefficient of the energy saving rate. An inconspicuous decline of energy saving rate but obvious decline of installation cost can be achieved when ω is 0.5. Therefore, the scheme when ω is 0.5 may be the preferable scheme achieving a compromise between better energy savings, voltage profile and lower installation cost. Their corresponding schemes are shown in Table 4.

Table 4. Conventional and optimized schemes of low traffic volume.

ω	TSS No.	1	2	3	4	5	6	7	8	9	10	11	12	13
1	Capacity [kWh]	5.5	6.0	7.0	6.0	4.0	3.0	3.0	4.0	4.0	4.5	5.5	5.0	6.0
	Power level [MW]	1.5	1.5	2.0	1.5	1.0	1.0	1.5	2.0	1.0	1.5	1.5	1.5	1.5
0.9	Capacity [kWh]	5.0	6.0	7.0	6.0	4.5	0	4.0	5.1	0	6.0	5.5	6.5	0
	Power level [MW]	1.0	1.5	1.5	1.0	1.0	0	1.0	1.5	0	1.5	1.0	1.0	0
0.5	Capacity [kWh]	0	7.0	7.0	6.5	0	0	5.5	0	0	6.5	0	6.5	0
	Power level [MW]	0	1.0	1.0	1.0	0	0	1.0	0	0	1.0	0	1.0	0

4.3.2. Moderate Traffic Volume

As seen in the second graph of Figure 21, when ω is 1.0, the best energy saving rate (9.8%) and regeneration cancellation rate (8.0%) can be obtained with installation cost of 8.94 M\$. When ω is 0.5, the energy saving rate decreases to 8.0%, the regeneration cancellation rate has not significantly changed, but the installation cost experiences a large decline from 8.94 M\$ to 4.16 M\$. Similarly, with a low traffic volume, we take the optimized scheme when ω is 0.5 as the reasonable scheme for ESS locating and sizing as shown in Table 5.

Table 5. Optimized schemes of moderate traffic volume.

ω	TSS No.	1	2	3	4	5	6	7	8	9	10	11	12	13
0.5	Capacity [kWh]	0	7.0	0	7.5	0	0	5.5	0	7.5	7.0	5.5	0	0
	Power level [MW]	0	1.0	0	1.5	0	0	1.5	0	1.5	1.0	1.5	0	0

4.3.3. High Traffic Volume

As seen in the third graph of Figure 21, when ω is 1.0, the best energy saving rate (1.88%) and regeneration cancellation rate (1.57%) can be achieved with an installation cost of 4.11 M\$. When ω is 0.5, the energy saving rate decreases to 1.43%, and the regeneration cancellation rate remains roughly stable, but the installation cost declines noticeably, from 4.11 M\$ to 1.52 M\$. Thus, we take the optimized scheme when ω is 0.5 as the preferable scheme, as shown in Table 6. From the table, the optimized powers and capacities under high traffic volume are much lower than that when they are under low and moderate traffic volumes.

Table 6. Optimized schemes of high traffic volume.

ω	TSS No.	1	2	3	4	5	6	7	8	9	10	11	12	13
0.5	Capacity [kWh]	0	0	2.0	2.0	0	0	2.0	3.5	0	0	0	1.5	0
	Power level [MW]	0	0	1.0	0.5	0	0	0.5	1.0	0	0	0	0.5	0

In the traditional configuration method, the capacity and power level of ESSs are generally determined by their maximum regenerative storage energy and peak power as shown of the above conventional schemes. However, some substations may present a high peak power but low mean power in certain traffic volumes, and under which circumstance there is no need to configure ESSs with a high power level, just as TSS4 shows whose peak power is 1.5 MW, but mean power is only 0.5 MW. After optimization, reasonable configuration schemes can be obtained with the most fitting power level.

4.3.4. Full Day Traffic Volume

According to the timetable provided by Subway Company, there are 19 h of running time in a full day including 3 h in low traffic volume, 6.5 h in moderate traffic volume and 9.5 h in high traffic volume, and based on which we can get the optimization trend as shown in the bottom right corner graph of Figure 21. Furthermore, its optimized scheme of full day when ω is 0.5 is shown in Table 7. In this case, the energy saving rate is 4.88%, the regeneration cancellation rate is 5.45%, and installation cost is 3.50 M\$.

Table 7. Optimized scheme of full day.

ω	TSS No.	1	2	3	4	5	6	7	8	9	10	11	12	13
0.5	Capacity [kWh]	0	8.0	0	5.0	0	0	5.5	0	0	8.0	0	5.0	0
	Power level [MW]	0	1.5	0	1.5	0	0	1.5	0	0	1.5	0	1	0

From the above optimized schemes, the optimized ESSs locations sometimes have a tendency to set in the substations with larger station spacing such as TSS4 and TSS7, but the concrete relationships between optimized locations and line conditions, including station spacing, slope and curve still, require further study.

4.4. Cost-Benefit Analysis

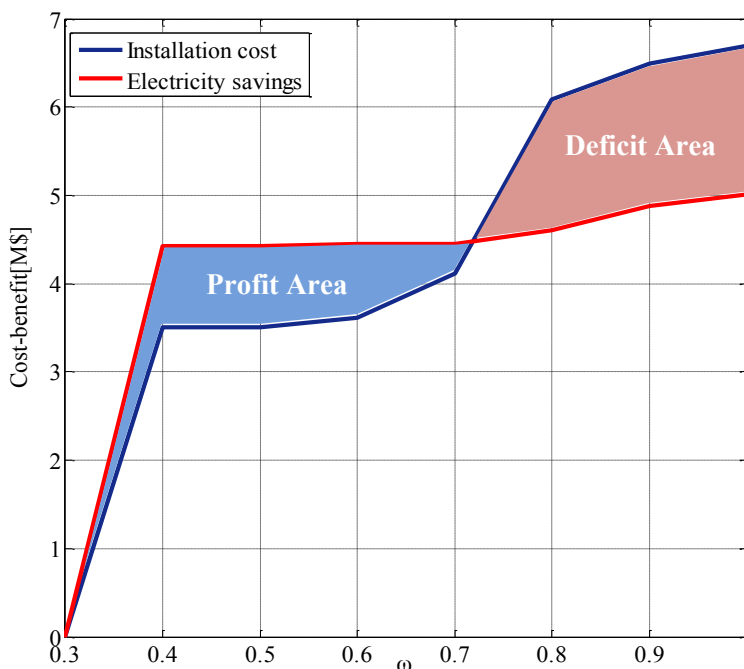
Combined with above full day optimization results, the electricity savings on the bills can be calculated as shown in the following formula.

$$M = E_{\text{consum}} \times \frac{E_{\text{rate}}}{100} \times Y \times P \tag{23}$$

where E_{consum} is the traction energy consumption per year when there are no ESSs set along the railway line; that is, 56.68 million kWh based on the simulation; while Y is the life of ultra-capacitors at room temperature, which we assume to be 10 years from [32]; and P is the price of electricity set as 0.16 \$/kWh.

In order to analyze the cost-benefit analysis, sensitivity analysis of installation cost and electricity savings for different ω , a full day has been analyzed in Figure 22. From the figure, when ω increases from 0.3 to 0.7, the benefits are greater than costs in the profit area. Especially when ω equals 0.4 or 0.5, the greatest profit of 0.9 M\$ can be obtained. When ω increases from 0.8 to 1, costs are greater than benefits in the deficit area, which is not recommended in application. If ESSs are installed, as Table 7 shows, with ω to be 0.5, and only considering the benefit from energy savings of substations, it will take about eight years to recover the installation cost.

Figure 22. Cost-benefit analysis diagram.



However, there are other potential benefits of ESSs that should be considered. On one hand, the installation of ESSs would develop the voltage profile, which can reduce the loss of brake shoes. Take the optimization scheme of full day for instance, the regeneration cancellation will decline from 14.69% to 5.45% after the installation of ESSs; thus, the replacement cycle of the brake shoe will last about 2.7 times as long. On the other hand, if brake resistors are set in convention lines, the addition of ESSs will reduce the tunnel temperature rise and reduce the secondary energy consumption of air conditions. Moreover, the energy savings, coupled with the system's ability to reduce CO₂ emissions, will contribute greatly to environmental preservation efforts.

5. Conclusions

The paper firstly raises the optimization objective functions from the perspectives of energy savings, regenerative braking cancellation and installation cost, respectively. Then, proper mathematical models of DC rail systems are established to simulate the electrical load-flow of the traction supply network, and also optimization objections are evaluated in the example of a Chinese metro line. Ultimately, a methodology for optimal ultra-capacitor energy storage system locating and sizing is put forward based on the improved genetic algorithm. The optimized results show that certain preferable schemes of ESSs' location and size can be obtained to equally satisfy the need for better energy savings, voltage profile and lower installation cost. By synthesizing all traffic conditions based on the timetable, we find an optimized scheme of full day with an average energy saving rate of 4.88%, a regeneration cancellation rate of 5.45%, and an installation cost of 3.50 M\$. Finally, the concrete profits of the optimized schemes in energy savings are verified by cost-benefit analysis.

Acknowledgments

This paper is part of projects supported by I13H100030 from Beijing Laboratory of Urban Rail Transit, I13H100020 from Beijing Key Laboratory of Urban Rail Transit Automation and Control, and I13L00100 from Beijing Subway.

Author Contributions

ZhongpingYang contributed to the conception of the study, Bin Wang contributed significantly to analysis and manuscript preparation, Fei Lin helped perform the analysis with constructive discussions and Wei Zhao provided the line and vehicle data.

Conflicts of Interest

The authors declare no conflict of interest.

References

1. Barrero, R.; Tackoen, X.; van Mierlo, J. Energy savings in public transport. *IEEE Veh. Technol. Mag. IEEE* **2008**, *3*, 26–36.

2. Barrero, R.; Tackoen, X.; van Mierlo, J. Improving energy efficiency in public transport: Stationary supercapacitor based energy storage systems for a metro network. In Proceedings of the Vehicle Power and Propulsion Conference, Harbin, China, 3–5 September 2008.
3. Ogasa, M. Energy saving and environmental measures in railway technologies: Example with hybrid electric railway vehicles. *IEEJ Trans. Electrical Electr. Engin.* **2008**, *3*, 15–20.
4. Ogasa, M. Onboard storage in Japanese electrified lines. In Proceedings of the 14th International Power Electronics and Motion Control Conference, Ohrid, Macedonia, 6–8 September 2010.
5. Hadjipaschalis, L.; Poullikkas, A.; Efthimiou, V. Overview of current and future energy storage technologies for electric power applications. *Renew. Sustain. Energy Rev.* **2009**, *13*, 1513–1522.
6. Ibrahim, H.; Ilinca, A.; Perron, J. Energy storage systems—Characteristics and comparisons. *Renew. Sustain. Energy Rev.* **2008**, *12*, 1221–1250.
7. González-Gil, A.; Palacin, R.; Batty, P. Sustainable urban rail systems: Strategies and technologies for optimal management of regenerative braking energy. *Energy Convers. Manag.* **2013**, *75*, 374–388.
8. Rufer, A. Energy storage for railway systems, energy recovery and vehicle autonomy in Europe. In Proceedings of the Power Electronics Conference (IPEC), 2010 International, Sapporo, Japan, 21–24 June 2010.
9. Steiner, M.; Klohr, M.; Pagiela, S. Energy storage system with ultracaps on board of railway vehicles. In Proceedings of 2007 European Conference on Power Electronics and Applications, Aalborg, Denmark, 2–5 September 2007.
10. Suzuki, T.; Hayashiya, H.; Yamanoi, T.; Kawahara, K. Application examples of energy saving measures in Japanese DC feeding system. In Proceedings of the 2014 International Power Electronics Conference (IPEC-Hiroshima 2014-ECCE-ASIA), Hiroshima, Japan, 18–21 May 2014.
11. Ciccarelli, F.; Del Pizzo, A.; Iannuzzi, D. Improvement of energy efficiency in light railway vehicles based on power management control of wayside lithium-ion capacitor storage. *IEEE Trans. Power Electron.* **2014**, *29*, 275–286.
12. Ciccarelli, F.; Iannuzzi, D.; Spina, I. Comparison of energy management control strategy based on wayside ESS for LRV application. In Proceedings of the IECON 2013—39th Annual Conference of the IEEE Industrial Electronics Society, Vienna, Austria, 10–13 November 2013.
13. Battistelli, L.; Iannuzzi, D.; Lauria, D. Energy management of electrified mass transit systems with energy storage devices. In Proceedings of the 2012 International Symposium on Power Electronics, Electrical Drives, Automation and Motion (SPEEDAM), Sorrento, Italy, 20–22 June 2012.
14. Iannuzzi, D.; Lauria, D.; Tricoli, P. Optimal design of stationary supercapacitors storage devices for light electrical transportation systems. *Optim. Eng.* **2012**, *13*, 689–704.
15. Iannuzzi, D.; Ciccarelli, F.; Lauria, D.; Clemente, G. An analytical solution for optimal design of stationary Lithium-ion capacitor storage device in light electrical transportation networks. *Int. Rev. Electr. Eng.* **2013**, *8*, 989–999.
16. Iannuzzi, D.; Ciccarelli, F.; Lauria, D. Stationary ultracapacitors storage device for improving energy saving and voltage profile of light transportation networks. *Transp. Res. Part C* **2012**, *21*, 321–337.
17. Barrero, R.; van Mierlo, J. Stationary or onboard energy storage systems for energy consumption reduction in a metro network. *J. Rail Rapid Transit* **2010**, *224*, 207–225.
18. Teymourfar, R.; Asaei, B.; Iman-Eini, H. Stationary super-capacitor energy storage system to save regenerative braking energy in a metro line. *Energy Convers. Manag.* **2012**, *56*, 206–214.

19. Iannuzzi, D.; Pagano, E.; Tricoli, P. The use of energy storage systems for supporting the voltage needs of urban and suburban railway contact lines. *Energies* **2013**, *6*, 1802–1820.
20. Bae, C.H.; Jang, D.U.; Kim, Y.; Chang, S.; Mok, J.K. Calculation of regenerative energy in DC 1500V electric railway substations. In Proceedings of the 7th International Conference on Power Electronics, Daegu, Korea, 22–26 October 2007.
21. Gildong, K.; Hanmin, L. A study on the application of ESS on Seoul metro line 2. In Proceedings of the International Conference on Information and Multimedia Technology, Jeju Island, Korea, 16–18 December 2009.
22. Hanmin, L.; Euijin, J.; Gildong, K.; Cheonheon, A. A study on the effects of energy storage system. In Proceedings of the International Conference on Information and Multimedia Technology, Jeju Island, Korea, 16–18 December 2009.
23. Hansang, L.; Hanmin, L.; Changmu, L.; Gilsoo, J. Energy storage application strategy on dc electric railroad system using a novel railroad analysis algorithm. *J. Electr. Eng. Technol.* **2010**, *5*, 228–238.
24. Jicheng, F.; Genson, J.; Yih-Kuen, J.; Jones, M. using artificial neural network to determine favorable wheelchair tilt and recline usage in people with spinal cord injury: Training ANN with genetic algorithm to improve generalization. In Proceedings of the 2011 23rd IEEE International Conference on Tools with Artificial Intelligence (ICTAI), Boca Raton, FL, USA, 7–9 November 2011.
25. Yao, X. Evolving artificial neural networks. *Proc. IEEE* **1999**, *87*, 1423–1447.
26. Guo, P.; Wang, X.; Han, Y. The enhanced genetic algorithms for the optimization design. In Proceedings of the 2010 3rd International Conference on Biomedical Engineering and Informatics (BMEI), Yantai, China, 16–18 October 2010.
27. Lv, G.; Sun, X.; Wang, J. A simulated annealing—new genetic algorithm and its application. In Proceedings of the 2011 International Conference on Electronics and Optoelectronics (ICEOE), Dalian, China, 29–31 July 2011.
28. Jiao, L.Y.; Lei, H.Z. The application of improved genetic algorithm in fitting the spatial variogram. In Proceedings of the 2011 International Conference on Computer Science and Network Technology (ICCSNT), Harbin, China, 24–26 December 2011.
29. Rodríguez-Díaz, F.J.; Garcia-Martinez, C.; Lozano, M. A GA-based multiple simulated annealing. In Proceedings of the 2010 IEEE Congress on Evolutionary Computation (CEC), Barcelona, Spain, 18–23 July 2010.
30. Shan, H.; Li, S.; Gong, D.; Lou, P. Genetic simulated annealing algorithm-based assembly sequence planning. In Proceedings of the Technology and Innovation Conference, 2006, Hangzhou, China, 6–7 November 2006.
31. Esbensen, H.; Mazumder, P. SAGA: A unification of the genetic algorithm with simulated annealing and its application to macro-cell placement. In Proceedings of the Seventh International Conference, Calcutta, India, 5–8 January 1994.
32. Datasheet: 125V heavy transportation module. Available online: http://www.maxwell.com/products/ultracapacitors/docs/125vmodule_ds_1014696-7.pdf (accessed on 3 July 2014).